

Mathematical Modeling and Designing a Heavy Hybrid-Electric Quadcopter, Controlled by Flaps

Mohammad Sadeq Ale Isaac^{*†}, Ahmed Refaat Ragab^{*‡}, Enrique Caballero Garcés[§],
Marco Andres Luna^{*†¶}, Pablo Flores Peña^{*}, Pascual Campoy Cervera[†]

^{*}Drone Hopper Company, Spain

[†]Polytechnic University of Madrid, Spain

[‡]University of Carlos III of Madrid, Spain

[§]UC3M and Aerodynamics Engineer at Drone Hopper

Systematic hybrid-electric unmanned aerial vehicles (UAVs) and, especially, quadcopters are so promising due to their long flight endurance and their usage in patrol and rescue missions which gain a high interest to be under examination and test scope by researchers; however, a complete mathematical design is required to fulfill theoretical complexities such as aerodynamic analysis and flight dynamics models related. This paper investigates salient sections from hypothesis to implementation. Researchers at Drone Hopper company have conducted various calculations to perform a precise novel platform called Duty-Hopper (DH). The benefit of this design is to control the attitude by flap vanes and electrical ducted fans (EDFs) when using gasoline engines; while, the principle propellers only lift the drone. This paper examines the attitude control system of DH, once using only flaps, then by only EDFs, and eventually, by compounding both. During this research, the scientific software used is ANSYS-Fluent and MATLAB-SimScape to analyze the entire body of the DH. Furthermore, a robust fault-tolerant controller is designed to immune the DH against internal and external errors. Our research reveals that using flaps is a feasible way to control attitude when it is augmented by EDFs.

Keywords: Hybrid-electric; UAV; quadcopter; duty-Hopper; EDF; flap.

1. Introduction

The hybrid-electric propulsion is a rather innovative technology system employed to combine the mechanical power generated by one (or more) electric drives with a thermal engine [7]. Hybrid-electric propulsive UAVs (HEP-UAVs) are highly valuable, thanks to removing heavy batteries and a long endurance; in counterpart, their disadvantage is the

control challenge. They perform beneficial applications such as wildfire fighting, long-term inspection, carrying heavy payloads, and patrolling UAVs [13,24]. There are various researches investigating HEP-UAVs. Bravo *et al.* [25] concentrated on the similarities and differences of the pure HEPs compared to conventional ones and introduced a normalized analysis to improve light HEP configuration, approaching the pure one. Savvaris *et al.* [26] worked on control and optimization of light HEP systems, using a parallel configuration architecture and supervisory control to implement in-ground hardware-in-the-loop (HIL) tests. Ruscio [27] emphasized the propulsion aerodynamics and wing mass of the fast general aviation class and validated it by implementing on double-engine Beechcraft 76 and the X-57 Maxwell to be in both propulsive and hybrid forms. Capata *et al.* [28] proposed a conceptual design of an

Received 27 May 2021; Revised 3 September 2021; Accepted 3 September 2021; Published 19 November 2021. This paper was recommended for publication in its revised form by editorial board member, Wen-Hua Chen. Email Address: marco.a@drone-hopper.com

This is an Open Access article published by World Scientific Publishing Company. It is distributed under the terms of the Creative Commons Attribution 4.0 (CC BY) License which permits use, distribution and reproduction in any medium, provided the original work is properly cited.

HEP-UAV feeding by ultramicrogas-turbine (UMGT), which powers an electric generator, concluding high-endurance flights, which is obtained by several aerodynamics analyses to optimize the specific fuel consumption. Nonetheless, Yung [16] made a survey on various propulsive and electric systems to compound an optimized simulated model, using both systems simultaneously, and according to this research, a HEP-UAV can save energy up to 6.5% compared to only a propulsive model. Throughout existing works, there is a gap for combining the theories and industrial form of HEP-UAVs. This research is undergoing to fill this space by presenting a rationale methodology and proving the statement. Generally speaking, HEP-UAVs require two completely independent systems which work simultaneously; thermal and electrical [16,24]. Principally, the system is powered by the gasoline engines, in which a shaft connects the rotating gears, and the main propellers maintain an adequate lift force to take-off, climb, and descend; however, this only relates to the throttle, since the gasoline engines do not respond abruptly, augmentation systems function for the rest of the control variables, including attitude values (ϕ , θ , and ψ) resulting in the lateral movement (x and y). This manner is better off, thanks to the gasoline motors, which make the HEP-UAV runway longer than electrical ones; however, this is mechanically complicated. There are various solutions, but the most efficient are variable-pitch governors or electric ducted fans (EDFs) to control the low-level control loop (attitude). Utilizing variable-pitch propellers as designated by Langkamp, [9], and Fresk in [18] requires an optimized point between pitch angle and motor RPM, which in the real world brings about many complexities such as controlling the swashplate rotation, internal errors of the pitch servos, and the gasoline engines. Furthermore, using servos for grand drones requires a long time of aerodynamics analysis to determine moments around blade hinges, then transforming to the pitch link and finally, find suitable servos. Therefore, it ought to concentrate on the latter technique, requiring less effort to harmonize the EDFs and choosing the best incident angle for the EDFs. Among all, Fan *et al.* [5] endeavored to demonstrate the attitude control efficiency using EDFs, which is an inspirable work; however, it needs a robust control method to prevent external errors and make the system traceable. Moreover, several researchers like [1,3,15,22] worked on the ducted fan solution, while all the works suffer from static instability of the model when flies, especially using flaps makes even the dynamic stability face problems. We have covered all aforementioned throats through this research by equipping the DH with four main ducts to move the center of mass (CoM) from the duct center to the quadcopter center, which causes the drone to fly stable. Actually, DH is considered as a powerful

HEP-UAV, which utilizes the technology of multiple flaps movement to be stabilized with minimum error; more specifically, to rotate toward the longitudinal, lateral, and vertical axis, it has eight distinct flaps pairwise. Considering redundant elements for stability and several control layers, DH has four coaxial pairs of propellers, 4 EDFs, 32 flap blades; i.e. every set of the rotor has four pairs, then to control rolling moment, longitudinal pairs works to have the moment stabilized; for pitching moment, lateral ones, and for yawing, the two diagonals vice versa. Regardless of redundancy, this schematic helps the system work undeniably safely; even if it loses some, others compensate for a complete movement. Such a design has various benefits such as being structured, immune and effortless; using mechanical systems instead of electric parts makes the DH user-friend. Notwithstanding rotors of conventional quadcopters produce all forces and moments, a very hasten response is considered a salient factor for distinct maneuvers; however, separating roles helps the system be more functionalized. In addition, redundant mechanisms could be controlled much more immune than the situation all-in-one. Besides, unwanted moments and energy are removed to improve the DH model; thanks to aerodynamic duct-tubes confined geometry, to somehow, the rotor moments are canceled out, especially during hover flight or maneuvers, flaps are operating, so the velocity of the main rotors is semi-conservative. Therefore, DH saves quite a lot of energy rather than similar cases without flaps. Another benefit of flaps is the static stability, helping the system to converge on the balance mode. While in most of the drones, propellers function as the main control targets, here instead, flaps and EDFs are employed to act as the attitude controller, and the fixed propellers only lift the drone, clustered as low-speed throttlers specified for quadcopters. Noting the novel controller employed is a robust sliding-mode that targets external errors to eliminate, which is highly required in the industry. This paper is arranged as follows. Section 2 clarifies a complete dynamic model of the DH. Section 3 discusses the implemented scenario. Section 4 reveals the results obtained. Finally, Sec. 5 compares the models expressed.

2. Dynamic Model of the DH

According to this research, the dynamic model of a large quadcopter is remarkably challenging because of plenty of internal errors that most of them are due to the difference among thermal engines characteristics even with the same model, such as their power causing sudden imbalances during flight. We have considered such problems in the

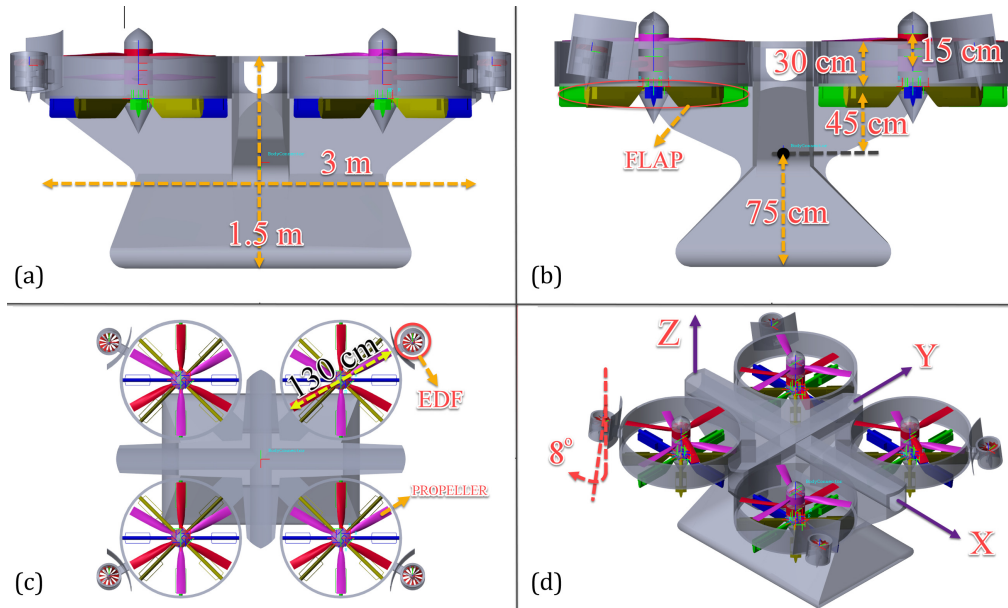


Fig. 1. A macroscopic schematic of the heavy DH. (a) side view; (b) toward or backward view; (c) up view; and (d) the 3D total vision of the DH.

virtual model by implementing unexpected random errors. A basic schematic of the DH is shown in Fig. 1. Various views of DH are revealed in this figure, including the vertical and horizontal dimensions (a); flap position, the center of mass (CoM), payload tank, and duct size (b); EDfs and four coaxial pairs of propellers (c); EDF angle of incidence, EDF wall, and *Body* frame (d). Inspiring from grand air-taxi *CityAirbus*. It is clear in Fig. 1(d) that the DH has four coaxial pairs of large propellers to lift principally; these eight propellers are augmented by four redundant EDfs to maintain the throttle safety margin in case of power-loss. Considering closed walls surrounding the EDF rotors, the vorticity throughout their ducts is semi-zero, producing an unimportant yawing moment. To compensate for this small magnitude, EDfs are installed with an incidence angle of 8°, and according to the experiments, normally, this angle is changeable up to 15° in case of high imbalance; however, DH has eight pairs of yaw flaps to maintain its stability; consequently, the inclination angle of EDfs is considered as 8°, which is the optimized angle, based on performed tests. While in Fig. 1(b), it is observed that CoM of the DH is [0 0 -0.45] Tm, the distance between CoM and bottom of the DH is 75 cm, and between the second propeller and the flap is 15 cm. In Fig. 1(c), the propeller diameter is 130 m and the EDF rotor diameter is 25 cm. Besides, the system has four 250 cc engines, with a total power output of 130 HP, which is equipped with a triple-redundant system. Considering the DH large body, all elements, even minuscule parameters have been under review. BTW, all equations are expressed in *Body* frame, supposing a

standard 6DOF system. The transitional equations of motion could be rewritten as in Eq. (1). This equation states the total external force, F^t , acting on the drone

$$F^t = \dot{m}v + m\dot{v} = F_x\hat{i} + F_y\hat{j} + F_z\hat{k}, \quad (1)$$

where v is the absolute velocity of the CoM. The first term of this equation states the mass ejection of the drone, which in the DH case is zero. Meanwhile, since the size of DH compared to the gravitational field is quite diminutive, the center of gravity (CoG) and CoM of the drone could be equal here. Extending the second term, the equation is as follows:

$$\begin{aligned} \dot{v} &= \dot{v}_r + wv \\ &= (\dot{u} + wq - vr)\hat{i} + (\dot{v} + ur - wp)\hat{j} \\ &\quad + (\dot{w} + vp - uq)\hat{k}, \end{aligned} \quad (2)$$

where ω is the absolute angular (rotational) velocity of the drone, \dot{v} and \dot{v}_r are absolute and relative accelerations of CoM, respectively. To summarize, gravitational, centrifugal, aerodynamic, rotors, and flaps forces and moments are expressed in the following equation, as is mentioned in [1]:

$$\begin{aligned} F^t &= F_{\text{grav}} + F_{\text{fuse}} + F_{\text{prop}} + F_{\text{duct}} + F_{\text{edf}} + F_{\text{flap}}, \\ M^t &= M_{\text{gyro}} + M_{\text{prop}} + M_{\text{duct}} + M_{\text{edf}} + M_{\text{flap}}, \end{aligned} \quad (3)$$

where F_{grav} is the gravity force affecting on the drone. Thereafter, all aforementioned forces and moments are described in six subcategories to show the effect of each parameter, i.e. gravitational force; aerodynamic forces; propeller force; duct force; flap force; and EDF force.

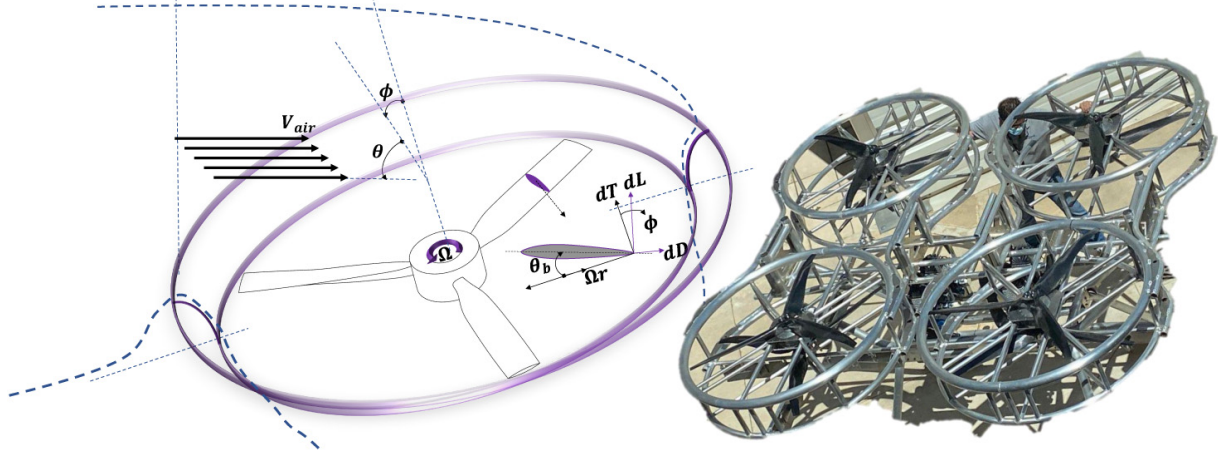


Fig. 2. Schematic of free-stream entering to the duct while inclined, where the real coaxial model is demonstrated.

2.1. Gravitational force and gyroscopic moment

Supposing the moving drone with θ angle toward the N -axis, ϕ angle toward E -axis, and ψ angle toward the D -axis, the third one does not affect on the gravitational force, then the equation is as follows:

$$\begin{aligned} \mathbf{F}_{\text{grav}} &= \begin{bmatrix} -mg \sin \theta \\ mg \cos \theta \sin \phi \\ mg \cos \theta \cos \phi \end{bmatrix}, \\ \mathbf{M}_{\text{gyro}} &= NJ\omega \begin{bmatrix} -q \\ p \\ 0 \end{bmatrix}. \end{aligned} \quad (4)$$

Related to the gyroscopic terms, N is the number of the propellers, J is the rotor inertia, p and q are angular rates of the propeller [1,5], regardless of aggressive behavior, this equation is supposed when the angular rates are semi-constant.

2.2. Fuselage forces

As a quadcopter, various components like fuselage, ducts, propellers, flaps, etc. produce reaction forces against the air passing throughout. Hereupon, drag force derived from the fuselage will be expressed through the following equation, as mentioned in [4,11]:

$$\mathbf{F}_{\text{fuse}} = -0.5\rho \begin{bmatrix} C_{D,x} u | u | A_{\text{side}} \\ C_{D,y} v | v | A_{\text{side}} \\ C_{D,z} w | w | A_{\text{top}} \end{bmatrix}, \quad (5)$$

where C_D is the drag coefficient of the fuselage, A_{side} is the cross area of the drone (here, regarding the symmetrical shape, both sides equal), and A_{top} is the top area of the drone.

2.3. Propeller forces and moments

The propeller is the principal thrust generator of the DH, entering free-stream air to the duct creating a boundary layer of inlet having a semi-circular shape [17]. If each propeller revolves with an angular velocity, the blade pitch θ_b , and the blade incidence angle ϕ_b , as shown in Fig. 2, this could be expressed as [8,9]. To calculate the thrust force generated by each propeller, the equation is as follows:

$$\mathbf{F}_{\text{prop}} = 0.5\rho A_r b \Omega^2 \begin{bmatrix} C_{D,b} \sin \alpha_b \sin \theta_b \\ -C_{D,b} \sin \alpha_b \sin \theta_b \\ C_{L,b} \cos \alpha_b \cos \theta_b \end{bmatrix}, \quad (6)$$

where Ω is the rotor angular velocity, b is the thrust factor of the propeller, and $C_{D,b}$ and $C_{L,b}$ are the drag and the lift coefficients of the propeller blades, and the A_r is the area of the rotor plane. Normally, θ_b and α_b are considered zero because of their small values.

2.4. Duct forces and moments

The propeller duct functions as an augmentative lifter when its lips are curved by aerodynamic extension. In addition, the closed walls of the duct to propellers, the fewer tip losses associated with free-air propellers. Due to ducts' inclination during the flight, they react to the air, and consequently, a momentum drag will be generated. When there is no crosswind (static condition), the momentum drag equals zero, since the stream enters the duct symmetrically; nonetheless, during movement, crosswind

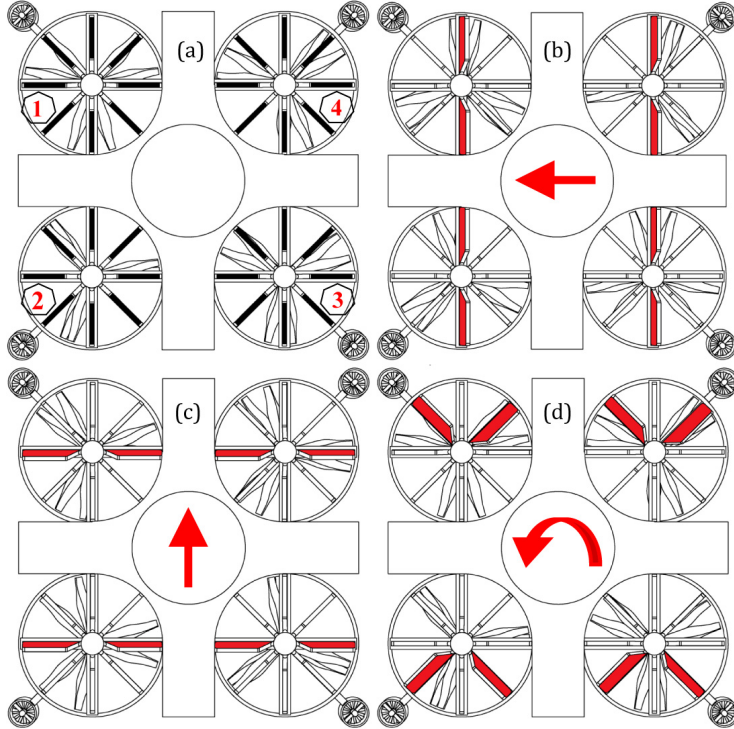


Fig. 3. Distribution of flaps movement; (a) hover mode without flapping, (b) four pairs of roll flaps are used to move toward y -axis, (c) four pairs of pitch flaps are used to move toward x -axis, (d) four pairs of psi flaps are used to rotate around z -axis.

enters asymmetrically [2,12]. Approximately, it could be given by

$$\begin{aligned} F_{\text{duct}} &= D_m + K_{\text{aug}} F_{\text{prop}} = 0.5 \rho C_d \begin{bmatrix} A_e V_{i,x} |V_{i,x}| \\ A_e V_{i,y} |V_{i,y}| \\ A_r K_{\text{aug}} V_r |V_r| \end{bmatrix}, \\ M_{\text{duct}} &= \begin{bmatrix} F_{\text{duct},y} r \\ F_{\text{duct},x} r \\ F_{\text{duct},z} l_d \end{bmatrix}, \end{aligned} \quad (7)$$

where K_{aug} is the augmentation factor of the duct helping propellers to trigger thrust, C_d is the duct moment coefficient which is a proportionality constant, in which the moment is related to the dynamic pressure due to cross-wind [1]. V_i is the inlet air velocity, r is the duct exit radii, l_d is the diagonal distance between the center of pressure (CoP) of the duct to CoG of the drone, and V_r , A_r , V_e , and A_e are the rotor plane and duct exit velocities and areas, respectively. Consider mass flow rate through the

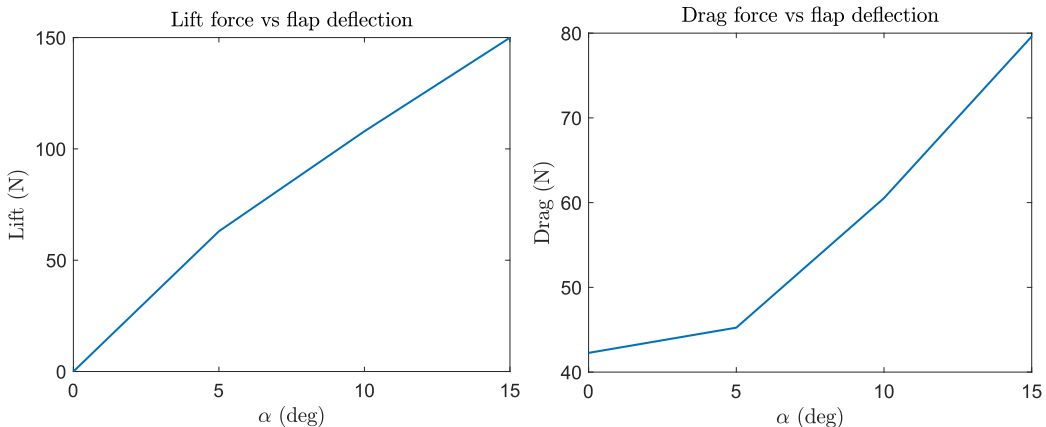


Fig. 4. Comparison of Lift and Drag forces versus increment of flap deflection angle.

duct [8,12,15]. In order to calculate the mass flow rate through the duct (\dot{m}_d), the following equation is used [3]:

$$\dot{m}_d = \rho A_i V_i = \rho A_e V_e. \quad (8)$$

2.5. Flap forces and moments

Regardless of incident angle or direction of installment, a flap can produce forces and moments in all coordinate axis [15]. Usually, flying drones use flaps to make the system more stable, preventing out-of-range moments; nevertheless, they have a standard form, hence for heavy drones, controlling by flaps is a big problem. That is why in grand systems, most flaps are employed as redundant components but not principles. The distribution of flaps movement is shown in Fig. 3, displaying the drone movement control to the right, left, upward, and backward.

In addition to the drone movement control, determining the calculation of a roll controller flap could be expressed as in Eq. (9), clarifying the roll flap force (F_{rf}) and the moment (M_{rf}) produced.

$$L = 0.5\rho V_e^2 A_e C_l,$$

$$D = 0.5\rho V_e^2 A_e C_d,$$

$$F_{rf} = \begin{bmatrix} 0 \\ L \cos \gamma - D \sin \gamma \\ L \sin \gamma + D \cos \gamma \end{bmatrix},$$

$$M_{rf} = \begin{bmatrix} M_x \\ M_y \\ M_z \end{bmatrix} = \begin{bmatrix} \pm F_{rf,z} dy_i - F_{rf,y} dz_i \\ \pm F_{rf,z} dx_i \\ \pm F_{rf,y} dx_i \end{bmatrix}, \quad (9)$$

Noting that L and D are the lift and drag forces generated by the flaps, γ is the deflection angle of each flap related to the vertical axis. During the flight, if $\gamma = 0$ no lift or drag is produced, and the more deflection angle is applied, the more lift is brought about. Meanwhile, the drag force is small enough. The research experiments demonstrate that for γ angles more than 18° , the increment rate of the drag force is more than lift, regardless of interference among flaps movements, and due to this fact result, it is observed that the best deflection angle domain is $0^\circ \leq \gamma \leq 10^\circ$, as presented in Fig. 4, which shows an increment of aerodynamic forces based on flap deflection angle when it rotates from 0° to 10° .

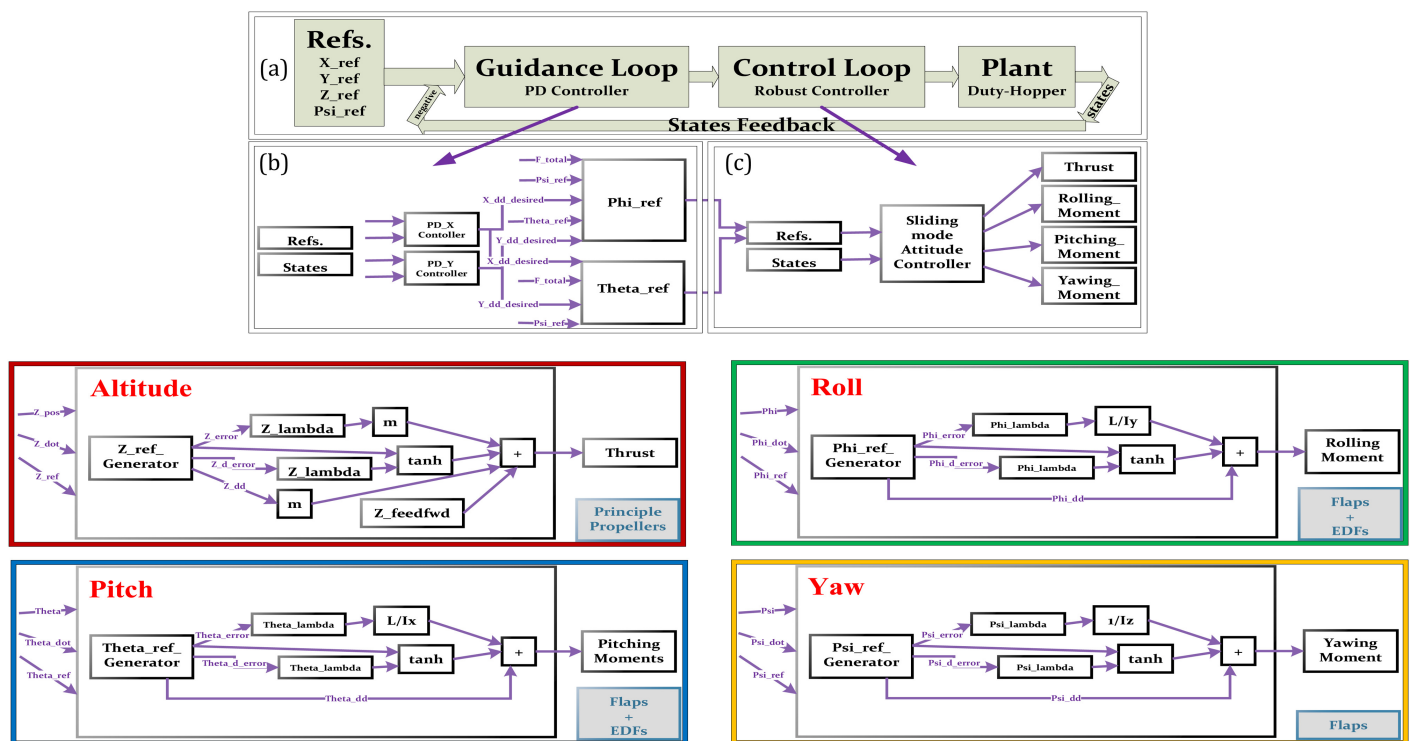


Fig. 5. A full schematic diagram of the guidance and controller loop to be simulated. Noticeably about the four squares below; thrust is produced by the main four pairs of propellers, rolling moment and pitching moment by flaps and in case of emergency aimed by EDFs, and yawing moment by flaps only. As described in Sec. 2, EDFs do not produce any magnificent yawing moment, especially here, they are installed inclined to cancel out each other.

Also, regarding to a pitch controller flap, Eq. (10) is given, presenting pitch flap force (F_{pf}) and its moment (M_{pf})

$$\begin{aligned} F_{pf} &= \begin{bmatrix} L \cos \gamma - D \sin \gamma \\ 0 \\ L \sin \gamma + D \cos \gamma \end{bmatrix}, \\ M_{pf} &= \begin{bmatrix} M_x \\ M_y \\ M_z \end{bmatrix} = \begin{bmatrix} \pm F_{pf,z} dy_i \\ \pm F_{pf,z} dx_i - F_{pf,x} dz_i \\ \pm F_{pf,y} dy_i \end{bmatrix}. \end{aligned} \quad (10)$$

Finally, for a determination of a yaw controller flap, the following equation is given, determining yaw flap force (F_{yf}) and its moment (M_{yf}):

$$\begin{aligned} F_{yf} &= \begin{bmatrix} \sqrt{2}/2(L \cos \gamma - D \sin \gamma) \\ \sqrt{2}/2(L \cos \gamma - D \sin \gamma) \\ L \sin \gamma + D \cos \gamma \end{bmatrix}, \\ M_{yf} &= \begin{bmatrix} M_x \\ M_y \\ M_z \end{bmatrix} = \begin{bmatrix} \pm(F_{yf,z} dy_i - F_{yf,y} dz_i) \\ \pm(F_{yf,z} dx_i - F_{yf,x} dz_i) \\ F_{yf,x} dy_i \pm F_{yf,y} dx_i \end{bmatrix}, \end{aligned} \quad (11)$$

where in Eqs. (9), (10), and (11), the sign \pm is observed alternatively, based on the nomination model.

2.6. EDF forces and moments

Like flaps, EDFs also are useful to make the drone more balanced. A normal formulation of an EDF rotor is likewise as propellers, but without considering lateral forces to conclude a drag or yawing moment. Instead, it produces a pure thrust with a much higher angular velocity rather than normal propeller engines. The EDF thrust equation can be stated as

$$\begin{aligned} \omega &= \sqrt{V^2 + (\pi d_r N)^2}, \\ \beta &= \arctan V / \pi d_r N, \\ F_{EDF} &= 0.5 \rho A_r b \omega^2 \begin{bmatrix} C_l \sin \beta + C_d \cos \beta \\ 0 \\ C_l \cos \beta - C_d \sin \beta \end{bmatrix}, \end{aligned} \quad (12)$$

where A_r is the surface area of the rotor plane, V is the blade axial velocity, N is the blade tangential velocity, β is the pitch angle of the blade, b is the thrust factor of the EDF rotors, and ω is the angular velocity of the rotor.

3. Implemented Scenario

Simulation tests, using MATLAB and practical tests of the DH model, are designed at Drone Hopepr to compare the

Table 1. DH detailed properties.

Part	Parameter	Range	Dimension
Fuselage	Mass	300	Kg
	Height	1.5	m
	Length/Width	3	m
	I_{xx}	337.32	Kg.m ²
	I_{yy}	337.32	Kg.m ²
	I_{zz}	466.84	Kg.m ²
	Number	4-Coax	—
Propeller	Number of Blades	3	—
	Nominal Rotor Rev.	1300	rpm
	Blade Radii	65	cm
	Blade Tip Chord	10	cm
	Blade Tip Angle	7	deg
	Thrust Factor [14]	2.15e-2	N · m ²
	Av. Damping Coeff.	0.05	N · m · s/deg
Propeller Servo	Number	4	cm
	Length	30	cm
	Outer Diameter	133	cm
	Inner Hub Diameter	155	cm
	Arc Radii at Tip	7	cm
	Av. Inlet air Velocity	135	m/s
	Av. Exit air Velocity	63.56	m/s
EDF	Number	4	—
	Number of Blades	12	—
	Nominal Motor Rev.	29000	rpm
	Blade Radii	12	cm
	Blade Chord	3.1	cm
	Blade Pitch Angle	45	deg
	Blade twist Angle	33	deg
EDF Servo	Thrust Factor	5.16e-6	N · m ²
	Av. Damping Coeff.	0.002	N · m · s/deg
	Number	4	cm
	Diameter	25	cm
	Arc Radii at Tip	1.6	cm
	Number	32	—
	Number per Prop	8	—
Flap	Height	14	cm
	Length	53	cm
	Av. Width	8	cm
	Maximum Angle	± 15	deg
	Av. Damping Coeff.	0.1	N · m · s/deg
	Number	32	—
	Number per Prop	8	—
Flap Servo	Height	14	cm
	Length	53	cm
	Av. Width	8	cm
	Maximum Angle	± 15	deg
	Av. Damping Coeff.	0.1	N · m · s/deg
	Number	32	—
	Number per Prop	8	—

data obtained. Through the scenario, a detailed schematic diagram system of the guidance and controller loops was designed, using Simulink and Simscape, as shown in Fig. 5. The simulation process was conducted in two steps, 3D modeling and compiling in aerodynamic and mechanical software (SW). First, during virtual reconstruction, each component is designed in Solidworks SW. Overall, there were more than 340 parts such as fuselage, propeller, EDFs and flaps. Every component is designed in detail to guide its actual model, and then this process is continued directly to prepare the simulation model. The DH complete detailed

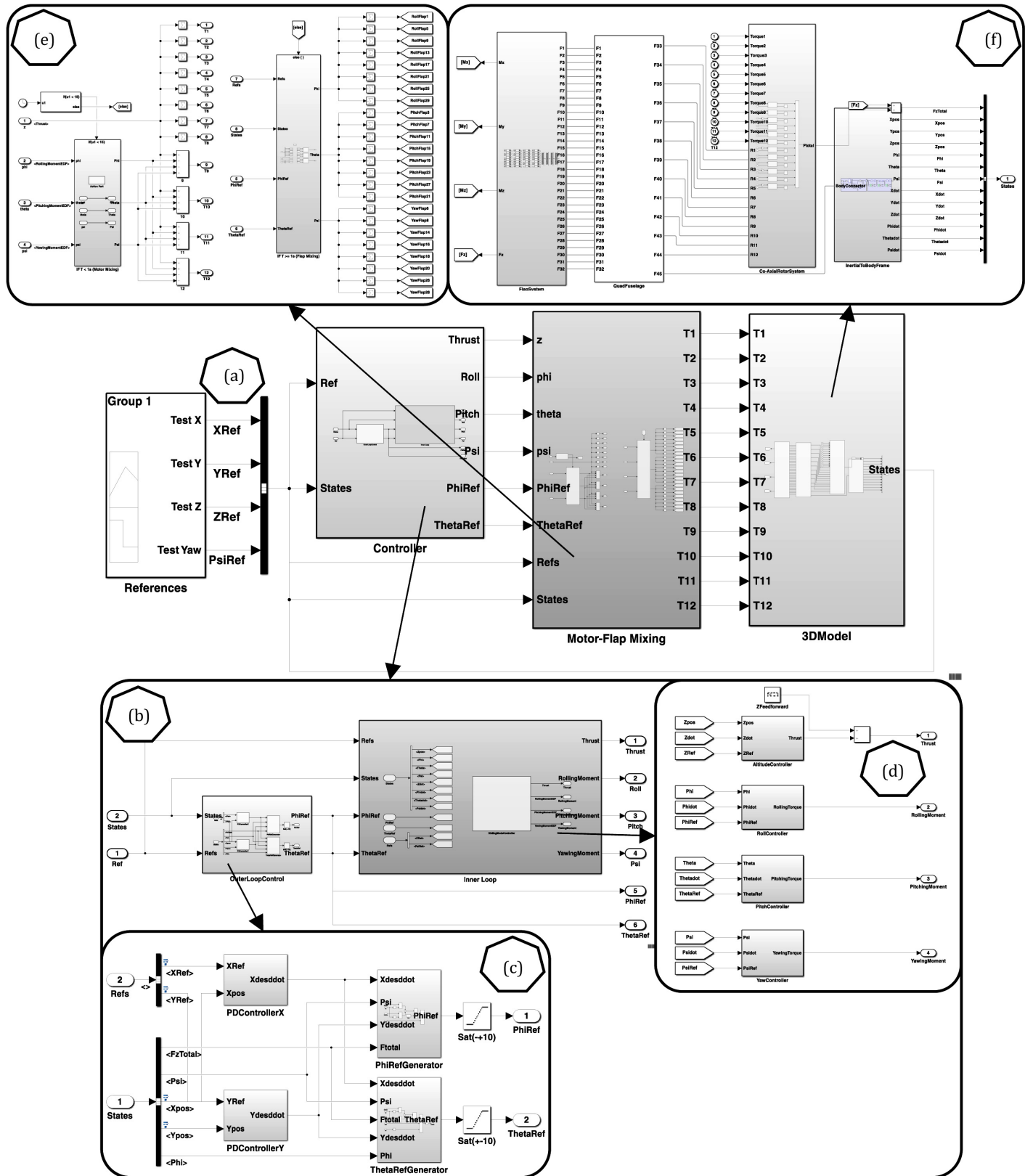


Fig. 6. A macroscopic schematic of the heavy DH simulation, using MATLAB Simulink.

properties are brought in Table 1. During the simulation, these magnitudes are changed several times to be optimized, and eventually, an accurate model is built. Meanwhile, to make the simulation appears realistic, various random noises are implemented, whether in local parts or from external phenomena, like internal errors in joints and wind disturbance models.

Second, ANSYS-Fluent and Simulink, as shown in Fig. 5, are used to analyze aerodynamic forces and moments, and DH behavior against disturbance. Simulink is a fully applicable mechanical platform to simulate forces and moments of objects. Here, the goal is to simulate the effective parts as a plant. Meanwhile, simulations of the DH in ANSYS-Fluent were done under the following setup, viscous model k-omega, transient (as the principle propellers are rotating), defining the cell zones materials (air for the enclosure and Carbon for the aircraft parts) and the moving parts rotating axis [10]. The boundary conditions were also set for the

inlet and outlet. Once the solution was obtained, the parameter Flap angle, previously created in the geometry editor SW, was varied in different design points to obtain the lift and drag forces on the flaps. Figure 5(a) demonstrates the overall configuration of the loops. Starting by denoting the four principle references (x_{ref} , y_{ref} , z_{ref} , and ψ_{ref}) which all inter into guidance loop (as the high level controller) and the results are generated ϕ_{des} and θ_{des} as indirect integrator inputs for the robust controller loop (as the low level controller). Finally, the controller outputs are applied to the plant besides feedback to complete the control diagram. Figure 5(b) presents the guidance part, containing two PD controllers. Based on this research, using a PD controller to generate attitude references values is optimized compared to when utilized PID; that is, using I brings about latency in the transient response. Equations used in this loop could be found in [6]. Furthermore, Fig. 5(c) shows the desired attitude parameters entering

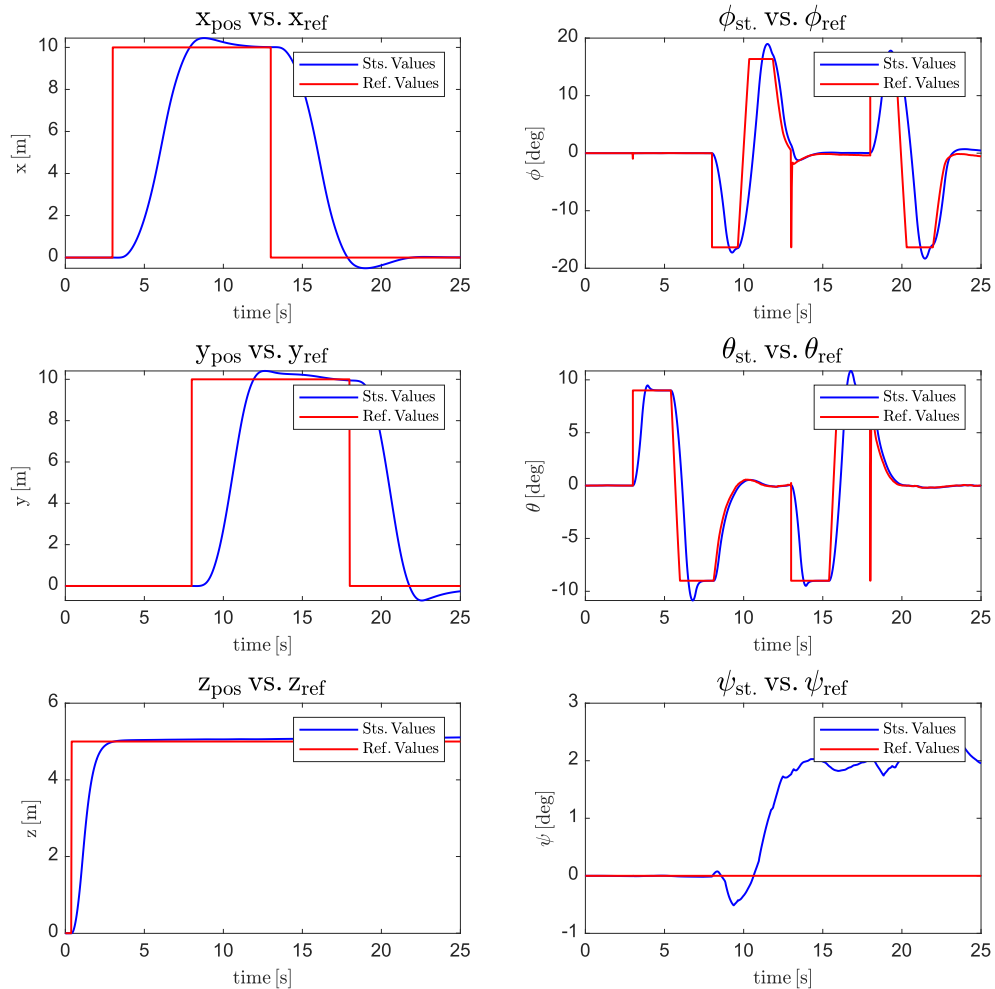


Fig. 7. Comparison of the drone state and reference positions and attitude angles, when $X_{\text{ref}} = 6 \text{ m}$, $Y_{\text{ref}} = 6 \text{ m}$, and $Z_{\text{ref}} = 5 \text{ m}$ and both flaps and EDFs are utilized.

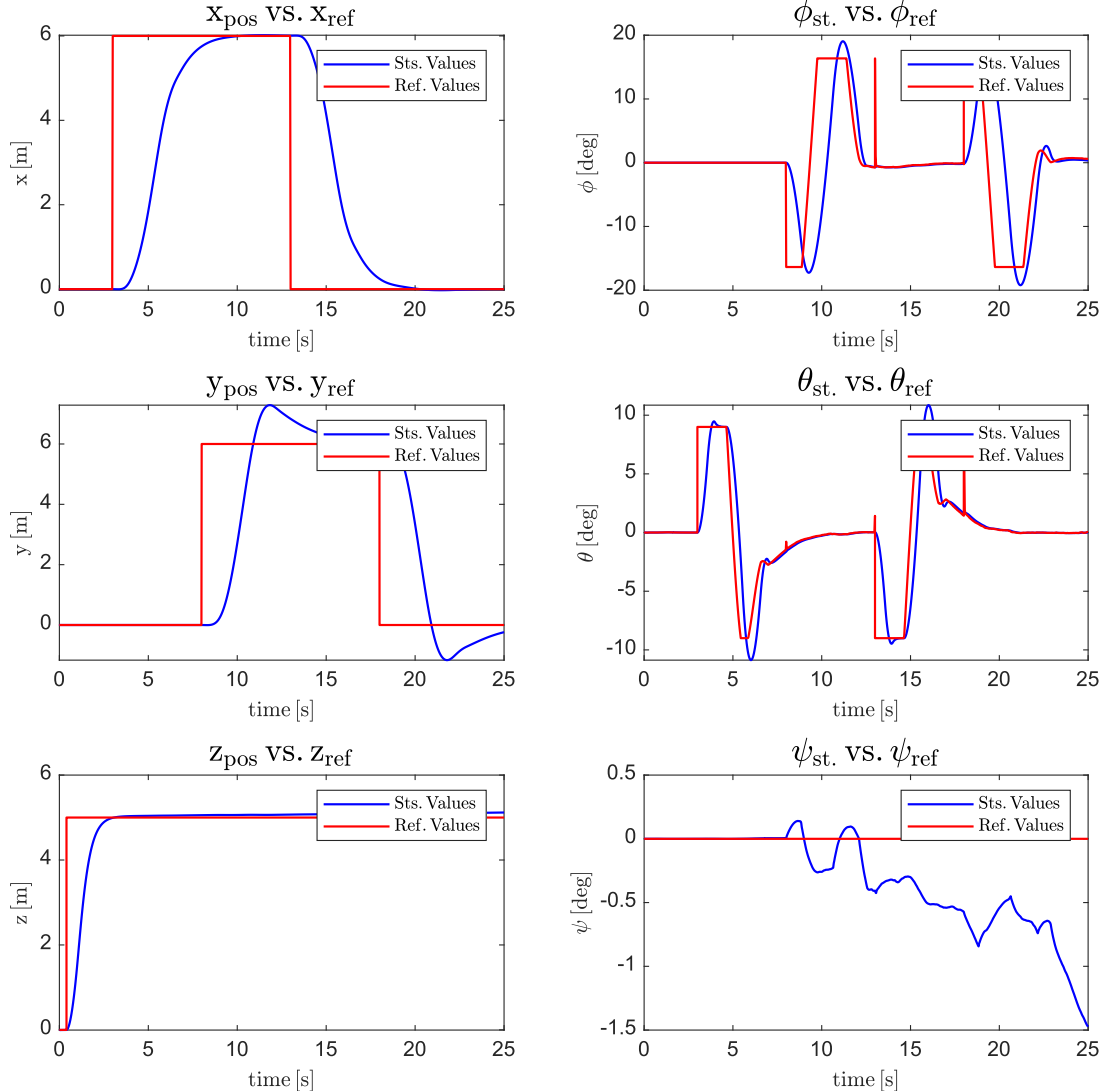


Fig. 8. Comparison of the drone state and reference positions and attitude angles, when $X_{\text{ref}} = 6 \text{ m}$, $Y_{\text{ref}} = 6 \text{ m}$, and $Z_{\text{ref}} = 5 \text{ m}$ and only EDFs are utilized.

into a low-level controller, denoting sliding mode is the robust method used in this work, then, all the attitude controller loops (including altitude loop) are mentioned and described below at Fig. 5(Altitude), 5(Roll), 5(Pitch), and 5(Yaw), which display the desired values computed by a reference generator (RG) box to generate saturated \ddot{z}_{des} , \dot{z}_{des} , Z_{des} , $\dot{\phi}_{\text{des}}$, $\ddot{\phi}_{\text{des}}$, $\dot{\theta}_{\text{des}}$, $\ddot{\theta}_{\text{des}}$, $\dot{\theta}_{\text{des}}$, $\dot{\psi}_{\text{des}}$, $\ddot{\psi}_{\text{des}}$, and $\dot{\psi}_{\text{des}}$ parameters. The aforementioned RG is a second-order system, which could be expressed as

$$G(s) = \frac{1}{s^2 + 2\xi\omega s + \omega^2}. \quad (13)$$

To continue, the sliding mode algorithm is deployed, this method could be formulated as in Eqs. (14), which concludes in thrust force (U_1), rolling torque (U_2), pitching

torque (U_3), and yawing torque (U_4)

$$\left\{ \begin{array}{l} \ddot{x}_d = -\lambda \dot{e}_x - K \tanh(S_x), \\ \ddot{y}_d = -\lambda \dot{e}_y - K \tanh(S_y), \\ U_1 = m(\ddot{z}_d - \lambda \dot{e}_z) - K \tanh(S_z), \\ U_2 = \frac{I_x}{l} (\dot{\phi}_d - \lambda \dot{e}_\phi) - K \tanh(S_\phi), \\ U_3 = \frac{I_y}{l} (\dot{\theta}_d - \lambda \dot{e}_\theta) - K \tanh(S_\theta), \\ U_4 = I_z (\ddot{\psi}_d - \lambda \dot{e}_\psi) - K \tanh(S_\psi). \end{array} \right. \quad (14)$$

Furthermore, in Fig. 5, where λ values are tunable like PID parameters, e_i is the difference between each value and

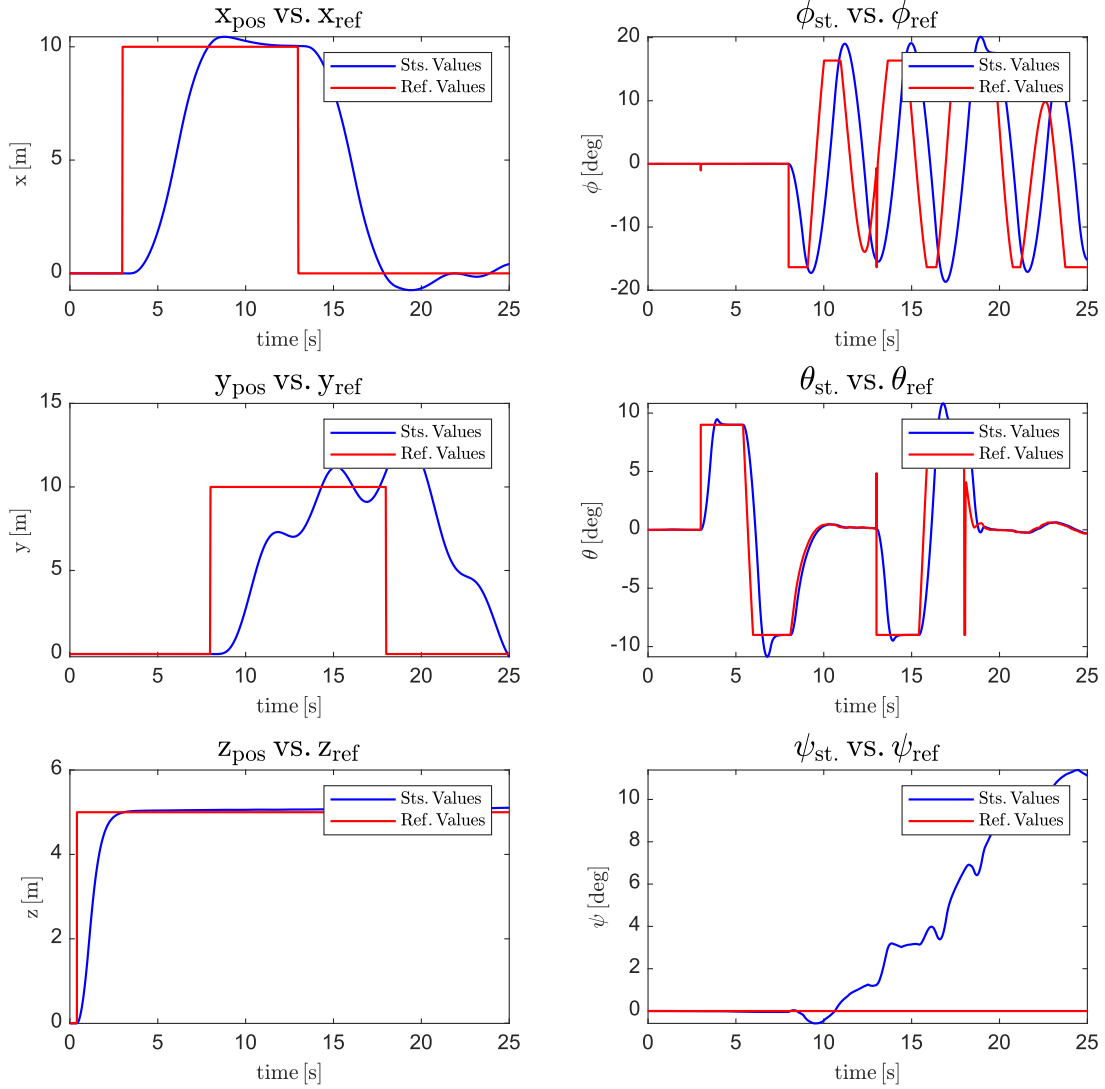


Fig. 9. Comparison of the drone state and reference positions and attitude angles, when $X_{\text{ref}} = 6 \text{ m}$, $Y_{\text{ref}} = 6 \text{ m}$, and $Z_{\text{ref}} = 5 \text{ m}$ and only flaps are utilized.

its reference, l is the length of the drone, K refers to a discontinuous component against system noises, which is calculated with try and error method; i.e. if it is more than a determined magnitude, the system will be stable. This is derived from the fact that how far negative is the Lyapunov function derivative, it will converge to a value more negative and so will be stable faster. In addition, instead of sign, we use the tanh function to make the chattering of the switching surface more smooth. As displayed in Fig. 5(d) and Eqs. (14), the output is a summation among position, velocity, and acceleration, where velocity is weighting element compared to others; consequently, to tune the controller, a higher amount is required to filter the velocity when goes out the integration. Likewise, Figs. 5(e), 5(f), and 5(g) show the attitude controller, denoting that yawing

torque is only produced by flaps; however, the roll and pitch moments could be generated using both. Figure 6(a) demonstrates the total configuration of the simulator, all of the main reference values are generated, using a signal producer; then controller part which is distributed into Fig. 6(b), regarded as the whole control loop. Considering higher level and lower level, once \dot{x}_{des} and \dot{y}_{des} are brought up, as shown in Fig. 6(c), by a PD controller to generate ϕ_{des} and θ_{des} [6], then entering reference and state magnitudes into the inner loop, the sliding algorithm is conducted to result thrust force and circular moments, as presented in Fig. 6(c). To continue, Fig. 6(e) displays the Motor-Flap Mixing part, which is the configuration of controller outputs to be legible for engines and flaps. As described in Fig. 5, the principle propellers are only in charge of generating lift

force, and for attitude, flaps and EDFs are employed. Finally, Fig. 6(f) demonstrates the 3D model of SimScape, which is imported from the previous approximated model in Solidworks. Despite the movements and rotations defined in modeler SW, here in counterpart, they are translated to *transform joints* and *revolut joints*, respectively, then a full 6DoF model is simulated by rotations to connect the *Body* and *Inertial* frames; therefore, all forces and moments are transformed. Moreover, a full model of 32 flaps, 8 EDFs, and the state feedback loop are developed in this segment.

4. Results and Analysis

Hereupon, some of the graph results are brought. Considering the mass is an important clue in such a heavy drone, then realize that it is impossible to tune a controller acting in a second. Meanwhile, through Fig. 5, it is cleared that the position and attitude variables are dependent, since the position values are issued by the reference block, and then through the guidance loop, attitude desired values (ϕ_{des} and θ_{des}) are computed. Despite a hasten reaction of small drones, the DH behavior is far slower. Figure 7 shows the comparison of the state and reference values of attitude angles, ϕ , θ , and ψ , when EDFs and flaps are working simultaneously. The minuscule yawing rotation is due to the unwanted moments affected on the drone, which is generated by increasing the damping coefficient of flap servos to accelerate and decelerate the yaw flaps abruptly. Figure 8 shows the comparison of the state and reference values of position, x , y , and z , when no flap functions and the drone is controlled only by EDFs. Supposing the command of the vertical axis is to go up to 5 m, and 6 m for the lateral values; hence, as described before, the DH acts latent but with less than 10% error is acceptable in graphs. Notwithstanding, the controller performance is semi-valuable using EDFs, controlling only by flaps makes the system highly delayed. This is due to the low power of flaps in such a grand system. Results in Fig. 9 demonstrate the impact of the flaps controller when no EDF is employed.

5. Conclusion

In short, during this research, once the system was designated to be controlled only by flaps, then only by EDFs, and finally, equipping both, concurrently. According to the results, it was observed that using only flaps makes DH suffer from latency as shown in Fig. 9. To the lower extent, when only EDFs work, the same phenomenon

was perceived. While equipping both flaps and EDFs makes the system acts agile, adequately, to be valuable in attitude control stability. Therefore, this research recommends using both flaps and EDFs in the control system. Moreover, the huge benefit of using such a system is controlling the attitude, using flaps and EDFs, and increasing the flight time endurance by using gas engines.

Acknowledgments

This project is pre-designed by the innovation group of Drone-Hopper company and implemented after a long-term simulation process in both propulsion and flight dynamics. We are thankful to all members who helped, especially Sebastián Álamo López, in parts of aerodynamics and flap controller.

References

- [1] E. N. Johnson and M. A. Turbe, Modeling, control, and flight testing of a small ducted fan aircraft, *J. Guidance Control Dynam.* **29** (2006) 769–779.
- [2] W. E. Graf, Effects of duct lip shaping and various control devices on the hover and forward flight performance of ducted fan UAVs, MS thesis, College of Aerospace Eng., Virginia Polytechnic State Uni., Virginia (2005).
- [3] M. Speck, J. Buchholz and M. Sellier, A mathematical model of a twin ducted-fan vertical takeoff and landing jetpack, *J. Aerosp. Eng.* **228**(10) (2013) 1831–1844.
- [4] J. Jeong, S. Kim and J. Suk, Control performance analysis on the variable configuration of ducted-fan flight array, *J. Aeronaut. Space Sci.* **21** (2019) 524–537.
- [5] W. Fan, C. Xiang and B. Xu, Modelling, attitude controller design and flight experiments of a novel micro-ducted-fan aircraft, *J. Adv. Mech. Eng.* **10**(3) (2018) 1–16.
- [6] M. S. Ale Isaac, S. H. Mirtajadini and A. Naghash, Control and guidance of an autonomous quad-rotor landing phase on a moving platform, in *IMAV Annual Conf. of Autonomous Vehicles* (Madrid, 2019).
- [7] L. Boggero, S. Corpino, A. D. Martin, G. Evangelista, M. Fioriti and M. Sorli, A virtual test bench of a parallel hybrid propulsion system for UAVs, *Aerospace, J. Aerosp.* **6** (2019) 77.
- [8] A. R. S. Bramwell, *Bramwell's Helicopter Dynamics*, 2nd edn. (Butterworth-Heinenmann, 2001).
- [9] D. Langkamp and W. J. Crowther, The role of collective pitch in multi rotor UAV aerodynamics, *36th European Rotorcraft Forum*, Vol. 1 (UK, 2010), pp. 238–245.
- [10] W. Graf, J. Fleming and W. Ng, Improving ducted fan UAV aerodynamics in forward flight, in *46th AIAA Aerospace Sciences Meeting and Exhibition* (Nevada, 2008), pp. 1–11.
- [11] M. A. Stamatte, A. F. Nicoleescu and C. Pupaza, Mathematical model of a multi-rotor drone prototype and calculation algorithm for motor selection, *J. Manufact. Syst.* **11** (2017) 119–128.
- [12] C. Xiang, W. Fan, H. Liu, B. Xu and N. Huang, Fan vehicle with tilting system, in *Int. Conf. on Unmanned Aircraft Systems* (Colorado, 2015), pp. 1196–1204.
- [13] S. Jafari, A. Bouchareb and T. Nikolaidis, Thermal performance evaluation in gas turbine aero engines accessory gearbox, *Int. J. Turbomach., Propul. Power* **5** (2020) 21.

- [14] P. Pounds, R. Mahony and P. Corke, Modelling and control of a large quadcopter robot, *J. Control Eng. Pract.* **18** (2010) 691–699.
- [15] Z. Wang, Z. Liu, N. Fan and M. Guo, Flight dynamics modeling of a small ducted fan aerial vehicle based on parameter identification, *Chin. J. Aeronaut.* **6** (2013) 1439–1448.
- [16] J. Y. Hung and L. F. Gonzalez, On parallel hybrid-electric propulsion system for unmanned aerial vehicles, *Prog. Aerosp. Sci.* **51** (2012) 1–17.
- [17] A. S. Sanca, P. J. Alsina and J. De Jesus, F. Cerqueira, Dynamic modeling with nonlinear inputs and backstepping control for a hexarotor micro-aerial vehicle, in *Proc. Latin American Robotics Symp. and Intelligent Robotics Meeting (LARS)* (Brazil, 2010), pp. 36–42.
- [18] E. Fresk and G. Nikolakopoulos, Experimental model derivation and control of a variable pitch propeller equipped quadcopter, in *IEEE Conf. Control Applications (CCA)* (France, 2014), pp. 723–729.
- [19] B. Wang and Y. Zhang, Adaptive sliding mode fault-tolerant control for an unmanned aerial vehicle, *J. Unmanned Syst.* **5**(4) (2017) 209–221.
- [20] E. Altug and A. Turkmen, A Novel mini jet engine powered unmanned aerial vehicle: Modeling and control, *Journal of Unmanned Systems, J. Unmanned Syst.* **1024** (2021) 012072.
- [21] Y. Xie, X. Zhang, L. Jiang, J. Meng, G. Li and S. Wang, Sliding-mode disturbance observer-based control for fractional-order system with unknown disturbances, *J. Unmanned Syst.* **8**(1) (2020) 1–10.
- [22] Y. Jin, Y. Qian, Y. Zhang and W. Zhuge, Modeling of ducted-fan and motor in an electric aircraft and a preliminary integrated design, *SAE Int. J. Aerosp.* **11**(2) (2018) 115–126.
- [23] C. L. Bowman, J. L. Felder and T. V. Marien, Turbo-and hybrid-electrified aircraft propulsion concepts for commercial transport, in *Proc. AIAA/IEEE Electric Aircraft Technologies Symp.* (USA, 2018).
- [24] S. Sahoo, X. Zhao and K. Kyriyanidis, A review of concepts, benefits, and challenges for future electrical propulsion-based aircraft, *J. Aerosp.* **7**(4) (2020) 44.
- [25] G. M. Bravo, N. Praliyev and Á Veress, Performance analysis of hybrid electric and distributed propulsion system applied on a light aircraft, *J. Energy* **214** (2021) 118823.
- [26] A. Savvaris, Y. Xie, L. Wang, S. Wang and A. Tsourdos, Control and optimisation of hybrid electric propulsion system for light aircraft, *J. Eng.* (2018) 478–483.
- [27] J. P. Ruscio, J. Jezegou, E. Benard, A. Gomez Pacheco, P. Laonet and R. A. Castilla, Hybrid electric distributed propulsion overall aircraft design process and models for general aviation (FAST GA), *IOP Conf. Ser.: Mater. Sci. Eng.* (2021).
- [28] R. Capata, L. Marino and E. Scibba, A hybrid propulsion system for a high-endurance UAV: Configuration selection, aerodynamic study, and gas turbine bench tests, *J. Unmanned Vehicle Syst.* **2** (2014) 16–35.



Mohammad Sadeq Ale Isaac is a robotic/aerospace Ph.D. student at the Polytechnic University of Madrid (UPM), Spain, and working as a control engineer at Drone Hopper Company, Madrid, Spain. He has been awarded his master's from Polytechnic University of Tehran (Amirkabir) in aerospace engineering, specializing in flight dynamics and control. His thesis is titled, "The autonomous landing of a drone on a chaotic moving platform". He mainly works on the nonlinear control field concentrated on flying drones.



Ahmed Refaat Ragab is a postdoctoral researcher at the University of Carlos III of Madrid (UC3M), Spain, and Drone Hopper Company, Madrid, Spain. He was a lecturer at October 6 University (O6U), Egypt. He graduated from Air Defense College, Alexandria, Egypt. His field of interest is Unmanned Aerial Systems.



Marco Andres Luna is a Ph.D. student at the Polytechnic University of Madrid (UPM), Spain and a software engineer at Drone Hopper Company, Madrid, Spain. He obtained his B.Sc. in automation and control engineering from Universidad de las Fuerzas Armadas ESPE, Ecuador, and his master's in automatic and robotics from the Polytechnic University of Madrid, Spain. His thesis' title was "3D location system for aircraft inspection by UAVs".



Pablo Flores Peña is an aeronautical engineer. He is the CEO and CTO of Drone Hopper Company, Madrid, Spain. He created the research center at Drone Hopper Company, Madrid, Spain. He also obtained a Master in Business Administration (MBA) at International Entrepreneurship (IE) Business School, Madrid, Spain. Previously, he was a chief engineer at Airbus Company, Spain, for more than 15 years.



Pascual Campoy Cervera is a professor at the Higher Technical School of Industrial Engineers of the Polytechnic University of Madrid (UPM), Spain. He is the head of the research group "Vision for Unmanned Aerial Vehicles (UAVs)" of the Department of Automation, Electrical Engineering and Electronics and Industrial Informatics, UPM. He belongs to the Center for Automation and Robotics, a joint research center of the UPM with the Superior Council of Scientific Investigations (CSIC). The objective of his research group is to provide unmanned systems with greater autonomy through the use of computer vision techniques.